



Coastal system evolution along the southeastern Caspian Sea coast using satellite image analysis: response to the sea level fall during 1994–2015

Ehsan Isaie Moghaddam¹ · Mohammad Nabi Allahdadi² · Ali Ashrafi³ · Nazanin Chaichitehrani²

Received: 8 November 2019 / Accepted: 12 April 2021 / Published online: 23 April 2021
© Saudi Society for Geosciences 2021

Abstract

The southeastern segment of the Caspian Sea (CS) along the Iranian coast, which has a very gentle inner shelf slope, underwent rapid beach evolution in response to water level changes. Based on satellite altimetry data, the CS basin has experienced an accelerated water level fall drop in recent years, leading to an increase in the rate of shoreline changes. The shoreline dynamics and morphodynamics of the Amirabad coastal zone, Gorgan Bay, Miankaleh Spit, and Gomishan Lagoon are evaluated here to determine morphological changes of the study area. Landsat-TM/ETM+/OLI moderate spatial resolution products were acquired at unequal intervals between 1994 and 2015 to monitor the coastal changes using Geographic Information System (GIS) tools. The Digital Shoreline Analysis System (DSAS), a GIS software extension, has been used for estimation of the shoreline rate of change through several approaches, including End Point Rate (EPR), Linear Regression Rate (LRR), and Weighted Linear Regression (WLR). The results show that both Gorgan Bay and Gomishan Lagoon have significantly decreased in size during recent years, mainly due to the fall of the CS water level. Results also show that water level drop of the CS, along with net eastward littoral transport, resulted in the growing of the Miankaleh Spit. Further analysis based on the wave climate in the southeast CS and net estimated longshore sediment transport indicates that the littoral drift contributed to ~6% of the total annual elongation of the Miankaleh Spit during the study period.

Keywords Caspian Sea · Gorgan Bay · Miankaleh Spit · Sea level changes · Landsat

Responsible Editor: Biswajeet Pradhan

✉ Ali Ashrafi
aashrafi@birjand.ac.ir

Ehsan Isaie Moghaddam
ehsan.isaiemoghaddam@gmail.com

Mohammad Nabi Allahdadi
mallahd@ncsu.edu

Nazanin Chaichitehrani
nchaich@ncsu.edu

- ¹ Fisheries Department of Sistan and Baluchestan Province, Chabahar, Iran
- ² Department of Marine, Earth, and Atmospheric Sciences, North Carolina State University, Raleigh, NC 27695, USA
- ³ Department of Geography, Faculty of Literature and Humanities, University of Birjand, University Blvd, Birjand, Southern Khorasan, Iran

Introduction

Coastal zones are commonly dynamic geomorphic environments that exhibit substantial spatial and temporal changes, especially in response to water level variations. Shoreline movements across a beach, morphological changes of barrier-lagoon systems, and beach-ridge emergence/submergence are common coastal responses to water level fluctuations in low-lying coastal segments (Kaplin and Selivanov 1995). The shoreline is the border between coastal land and the water body. However, identification of the shoreline can be challenging. Because of the natural variability of water level, climatologic conditions, the effects of coastal processes including sediment transport by wave-induced currents, and human interventions on beach platforms, shoreline position varies continuously through time (Bartlett and Smith 2004; Boak and Turner 2005; Liu et al. 2013; Isaie Moghaddam et al. 2018; Chaichitehrani et al. 2019). Thus, studying coastline changes is essential for coastal zone management, environmental protection, and sustainable

development (Aedla et al. 2015; Zuzek et al. 2003). Various data sources such as coastal maps and charts, beach surveys, and aerial photographs are employed for shoreline change analysis (Boak and Turner 2005). During recent decades, satellite remote sensing technology has been a reliable tool for mapping shoreline changes over large spatial scales (Liu et al. 2013; Vinayaraj et al. 2011).

The application of remotely sensed data for studying shoreline change in coastal regions has been presented in many publications. Aedla et al. (2015) studied beach variations on the west coast of India by developing histogram equalization and adaptive thresholding techniques to detect the shoreline automatically. The delineated shorelines were examined using the Digital Shoreline Analysis System (DSAS) for estimation of change rates through two statistical approaches: End Point Rate (EPR) and Linear Regression Rate (LRR). Kuleli et al. (2011) analyzed shoreline changes along the coastal Ramsar wetlands of Turkey using segmentation algorithms for automatic extraction of the coastline using multi-temporal Landsat images. The study of Kermani et al. (2016) is an excellent example of using a long-term time series of satellite images to delineate shoreline changes. They analyzed historical shoreline change trends along the beaches of Jijel (East Algeria) between 1960 and 2014 from multi-dated aerial photos and Quick-bird satellite images. The shoreline position and evolution were detected by manual digitization technique (wet/dry line proxy). Further, EPR, LRR, and Weighted Linear Regression (WLR) statistical approaches were used for evaluating the long-term rate of shoreline movement. Kourosh Niya et al. (2013) employed a new semi-automatic approach to map coastline changes of the Persian Gulf throughout 1990 to 2005 utilizing histogram threshold and band ratio techniques. Use of the band ratio techniques was one advantage of their study, making it possible to select a threshold for defining land and water boundaries.

Several studies addressed coastal morphology response along the Caspian Sea (CS) to water level variations. Rasuly et al. (2010) evaluated the integration of object-oriented and pixel-based techniques for monitoring the evolution of a part of south CS shoreline from Landsat MSS, TM, and ETM images of the past three decades. Kakroodi et al. (2014) studied both landward and seaward shifts during rapid sea level rise between 1977 and 2001 along the Iranian coast of the CS using different Landsat data and the edge enhancement technique for extracting shoreline. In a recent study, Gharibreza et al. (2018) studied Gorgan Bay's evolutionary trend in the southeast CS produced by the last sea level rise from 1977 to 1995 using satellite images and sedimentology data. They concluded that the sea level rise reinforced the sedimentation at the entrance and inside the basin of Gorgan Bay. The historical records of CS water level show that during recent decades it has experienced both sea level rise and fall. As mentioned above, morphological aspects as consequences

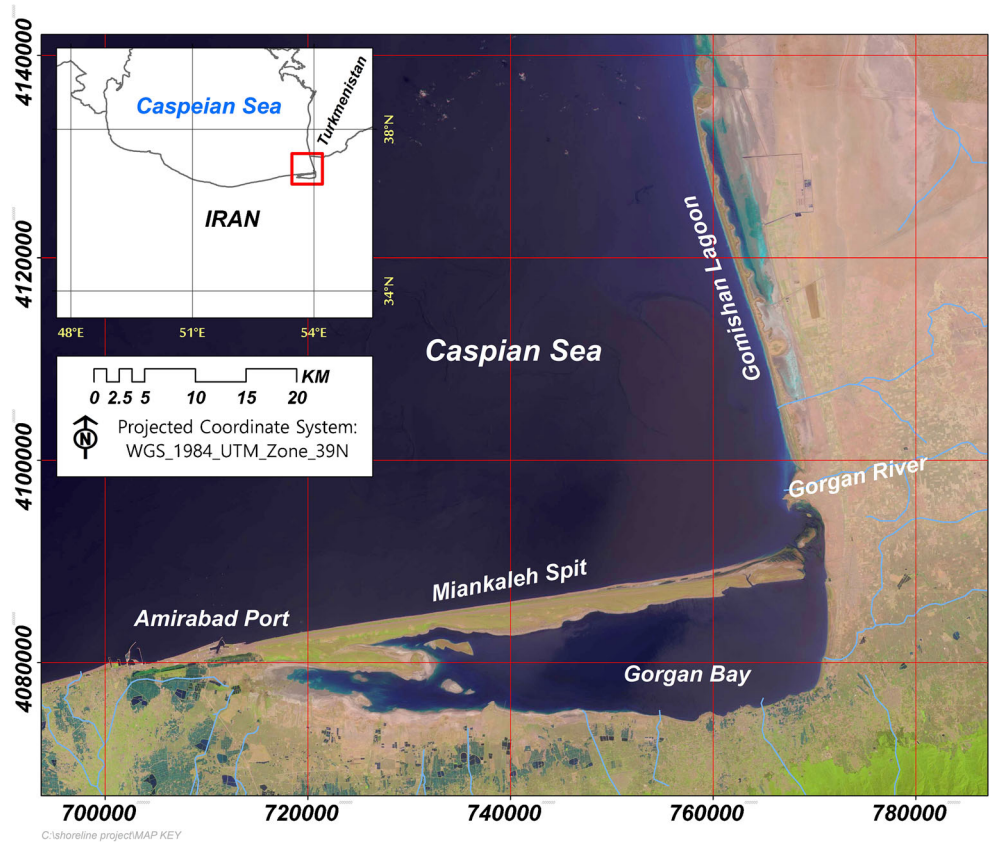
of sea level rise in the southeast CS have been addressed by several studies, while the impacts associated with sea level drop have been less studied.

This paper is one of the first attempts to quantify and discuss the changes driven by sea level drop along the southern coast of the CS. In this study, Amirabad Coastline, Miankaleh Spit, Gorgan Bay, and Gomishan Lagoon along the southeastern CS coast have been chosen for investigation of shoreline evolution caused by natural and anthropogenic processes utilizing satellite image analysis and statistical methods during different periods in the past. The focus is on the recent sea level drop during 1994–2015. Morphological changes of selected regions have been quantified in terms of size and surface area to evaluate shoreline changes further. The main objective is to understand better the factors that control shoreline change patterns and morphological aspects of the study area.

Study area

The study site is located on the southeastern coast of the CS (Fig. 1). The CS is the world's largest enclosed water basin. Although the CS is isolated from the open sea, due to its other characteristics, including large size, great depth of water, the occurrence of severe gales, and a specific hydro-chemical regime, it is classified as a deep inland sea (Lebedev 2004). This makes the CS the world's largest lake, containing 44% of inland water globally (Ibrayev et al. 2010). The 2015 level of the CS was around -27 m relative to open ocean mean sea level. The sea occupies an average area of 392,600 km² and has a semi-elliptical basin oriented in a north-south direction with a length of ~ 1200 km and a mean width of ~ 310 km (Kosarev et al. 2012; Leroy et al. 2009). The CS includes three zones with varied depths and oceanographic characteristics: the north Caspian (maximum water depth ~ 20 m), the middle Caspian (water depths up to 788 m), and the south Caspian (water depth up to 1025 m). The south basin contains nearly two-thirds of the total water volume in the CS (Kaplin and Selivanov 1995). The CS is virtually tide free, and its entire coastline is ~ 4460 km. The Iranian Caspian coastline extends from the southeast to southwest with a total length of ~ 800 km (Leroy et al. 2009; Naderi Beni et al. 2013). Within the last century, the CS underwent dramatic sea level fluctuations so that the water level oscillated with an amplitude of ~ 3 m between 1929 and 1995. According to water level observations, its sea level was relatively stable between 1880 and 1929, fluctuating around a mean of -26 m (Fig. 2; Lepeshevkov et al. 1981; USDA 2015). A substantial decrease (1.6 m) in CS level began in 1930, and the sea level was as low as -27.7 m in 1940. The rate of sea level decline was slower after 1940, exhibiting a 1.4 m drop in 37 years. At the end of this period in 1977, the sea level decreased to -29.1 m (Firoozfar et al. 2012). This drop is considered the largest in

Fig. 1 Location of the study area



the last 400 years (Rychagov 1997). From 1977 onwards, it increased once again to reach pre-1930s levels (−26.7 m). Recent satellite altimetry data from TOPEX, JASON, and Ocean Surface Topography Mission (OSTM) demonstrated that the CS water level reached a high in 1995 with a small rise in 2005 and a large rate of fall from 2011 onwards (Kakroodi et al. 2014) (Fig. 3). Overall, the general trend from 1995 to 2015 was a drop in sea level. The water level variations in the CS are mainly a function of changes in the total river inflow (the Volga River discharges 80% of total water flow into the CS), the outflow from the CS to Kara-Bogaz-Gol Bay, precipitation, groundwater runoff, and evaporation (Lebedev et al. 2008).

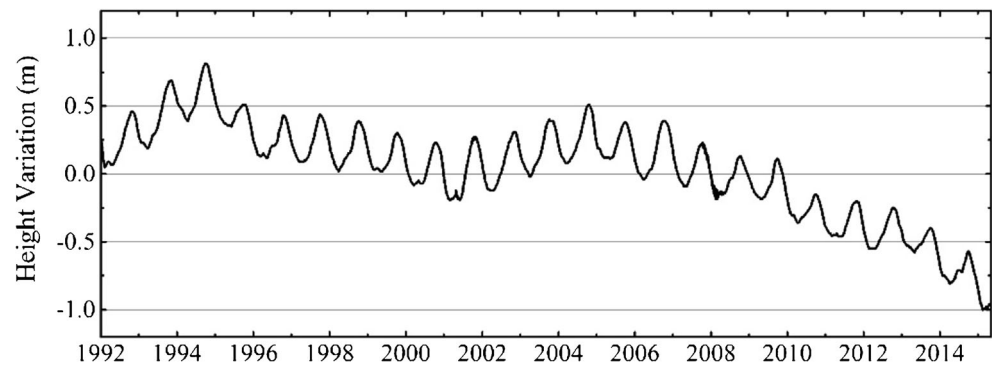


Fig. 2 Instrument-observed Caspian Sea level (in meters) relative to open ocean mean sea level during the period 1880–2010

The study sites encompass part of the Iranian coast along the southeast CS, including the Amirabad Coastline, Gorgan Bay, Miankaleh Spit, and Gomishan Lagoon (Fig. 1). These regions are recognized as areas with high volumes of industrial and economic activities and are of great importance for marine resources, ecological variety, and tourism. The southeastern Caspian coast is characterized by varied landforms and geomorphological features like mainland shores, deltaic coasts, barrier islands, and spit-lagoon systems. Since tide in the CS is negligible (Terziev 1992), coastal processes and beach morphology are predominantly influenced by sea level changes, waves, and coastal currents. The Gorgan Bay and Gomishan Lagoon are the major geomorphological features along the southeastern CS coast, formed behind the barrier beaches and separated from the CS by spits (Lahijani et al. 2009). In this coastal zone, waves approach mainly from the northwest and north (Terziev 1992). The highest waves occur during the winter, when they can reach a significant height of up to 2.25 m (Pourmandi Yekta et al. 2010; Allahdadi et al. 2004). However, most of the year, wave height is less than 1 m. Therefore, the southeastern CS coast can be considered a dissipative low-energy environment (Lahijani 1997; Voropaev et al. 1998).

Due to the dominant wind and wave directions, the net littoral drift along the southeast CS coast is to the east (Gharibreza et al. 2018). In the southeastern CS, the closure

Fig. 3 Long-term water level variation of the CS, based on TOPEX/POSEIDON, JASON-1, and JASON-2/OSTM altimetry data between 1992 and 2016



depth point is far from shore owing to the low beach gradient that prevents high waves from approaching the shore. Hence, the coastal bed material is composed mainly of fine-grained sediments.

The Gorgan River system (Fig. 1), the highest-volume river feeding the southeastern CS, begins its course from Kopet Dag Mountain (on the border between Turkmenistan and Iran) and discharges annually ~ 407 million m^3 of water and 2.15 million tons of sediments to the coast (Alizadeh Ketek Lahijani et al. 2008). The region's climate is semi-arid, with average annual rainfall of 437 mm and average relative humidity mostly above 73% (Lahijani et al. 2009). Sea surface temperature varies in winter between 7 and 10 °C while the range in summer is 25–29 °C (Ibrayev et al. 2010). Winds from the northwest and north dominate most of the year (Allahdadi et al. 2004).

Materials and methods

Datasets

The study area's coastal changes were monitored with satellite images, including Landsat 4 and 5 TM, Landsat 7 ETM+SLC-on, and Landsat 8 OLI. In this study, a series of images were obtained from the US Geological Survey (USGS; <http://earthexplorer.usgs.gov>) with a pixel size of 30 m spanning 1994 to 2015. Images were corrected with the aid of Standard Terrain Correction. They were converted to radiometrically and geometrically terrain-corrected data that made them suitable for time series analysis. The georegistration is consistent and within prescribed tolerances (Root Mean Squared Error (RMSE) < 12 m; <https://landsat.usgs.gov>). Images utilized in this research are as follows:

1. Landsat 4-5 TM images (101 sets) at non-uniform time intervals between September 21, 1994, and October 6, 2011, 45% of which were cloud-free and usable over the whole study region.

2. Landsat 7 ETM+SLC-on sensor images (38 images) from July 9, 1999, to May 17, 2003. Nearly 39.5% of the collected images had no cloud cover and were used to analyze coastal variation. Although many images from Landsat 7 ETM+SLC-off sensor products were available, these images were only suitable for the Gomishan area and had dark stripes and poor quality in other regions.
3. Landsat 8 Operational Land Imager (OLI) images (66 data products, available at the US Landsat data archive) for the study area. 42.5% of the products contained low cloud cover so were employed in the study.

The effect of cloudiness and contamination of images by sun glare (causing the appearance of dark stripes in the images) significantly limits the number of suitable images and the historical time series for shoreline delineation. Hence, in the final study database, the time intervals between the images are not uniform.

Image processing and shoreline demarcation

As the first stage for detecting shoreline from the selected satellite images, atmospheric corrections were applied using the FLAASH module of ENVI. Multi-temporal satellite images were georeferenced through image-to-image registration. The average RMSE associated with these corrections was generally kept to less than 0.5 pixels. Corrected images were loaded for demarcation of the shoreline using two approaches: histogram thresholding on band 4 and the band ratio method. Further comparisons and investigations showed that band 4 thresholding results in higher accuracy land-sea boundaries for the study area. The image histogram associated with this band includes a sharp, double-peaked curve. The threshold value between the peaks was calculated using the JENKS natural breaks classification method. This method is applied to segregate sea from land. One challenge in applying this method for our study area is the gentle slope of the seabed and coastal region and the variety of the coastal landforms. This challenge makes the determination of the exact threshold value based on only one band difficult. Hence, following

Kourosh Niya et al. (2013), the ratio between bands 5 and 2 and bands 4 and 2 were used to improve accuracy. It should be noted that each band of Landsat represents the reflected signal at a specific wavelength. Therefore, the band ratio shows the ratio between the reflectance corresponding to two distinct wavelengths. Whenever high-quality true color images of the study area were available, they were used as the ground truth to differentiate between land and water. Otherwise, the band ratio method was used for more accurate segregation. Figure 4 shows an example map for the land and sea segregation based on the band ratio method explained above.

Estimation of shoreline position error

To enhance the accuracy of shoreline extracted using the above approaches, the very high-resolution satellite imagery offered by Google Earth Pro was used. To identify the shoreline across the study area, a high-pass filter technique was applied on georeferenced images (all images were georeferenced with Ground Control Points). The RMSE associated with these corrections was generally less than 1 m. Five control points were used to check the calculations' validity for each of the three parts of the study area (Gorgan Bay,

Amirabad Coastline, and Gomishan Lagoon). Different threshold values on band 4 of multi-temporal Landsat images were applied to map the shoreline. The accuracy of the derived shorelines close to the control points was subsequently assessed.

After applying ten iterations for each image and calculating RMSE for each of them, the iteration corresponding to the smallest RMSE was used as the threshold for shoreline demarcation that included converting raster to vector layers. The deduced shorelines were smoothed using the PAEK algorithm, and different layers were prepared for calculating the rate of shoreline change. A summary of the data and methodology adopted in this study is presented in Fig. 5.

Calculation of shoreline change rate

Statistics for the rate of change are commonly computed to identify a coastline's behavior and the processes that have affected the coast over time. To analyze the dynamics of shoreline movements and changes in the study area, the DSAS software version 4.3, an extension developed by the USGS, was used. DSAS computes the rate of change statistics for a time series of shoreline positions.

Fig. 4 **a** An example of land and sea differentiation based on the ratio of bands 5 and 2. **b** The image based on the false-color representation of bands 3, 4, and 5 of Landsat. **c** A close view of **b**

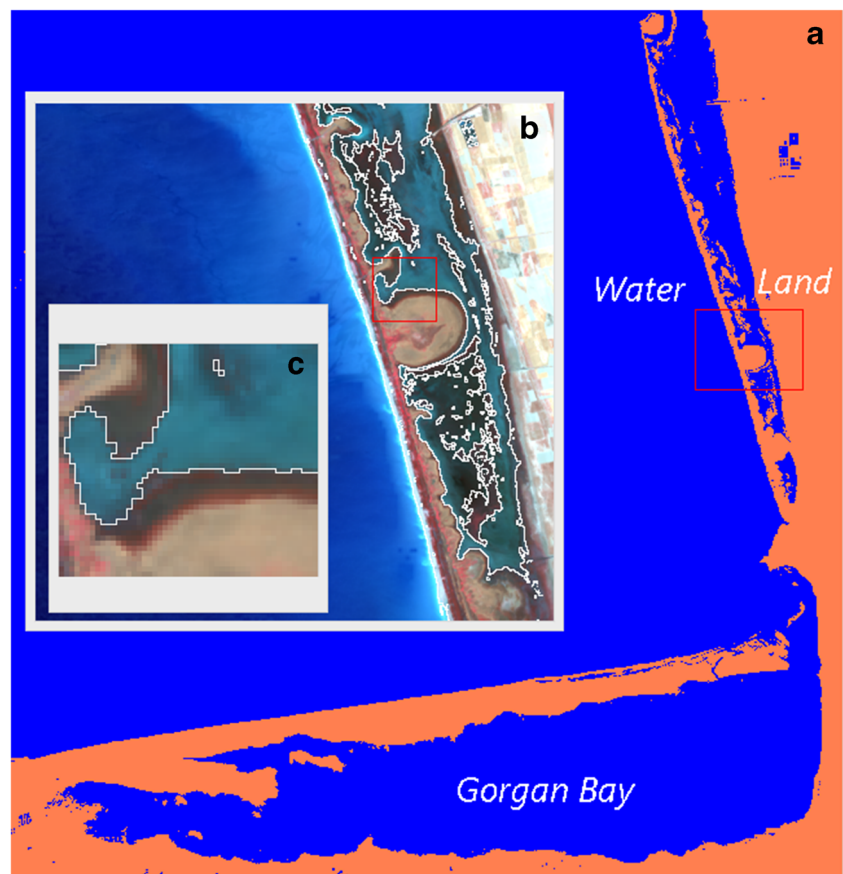
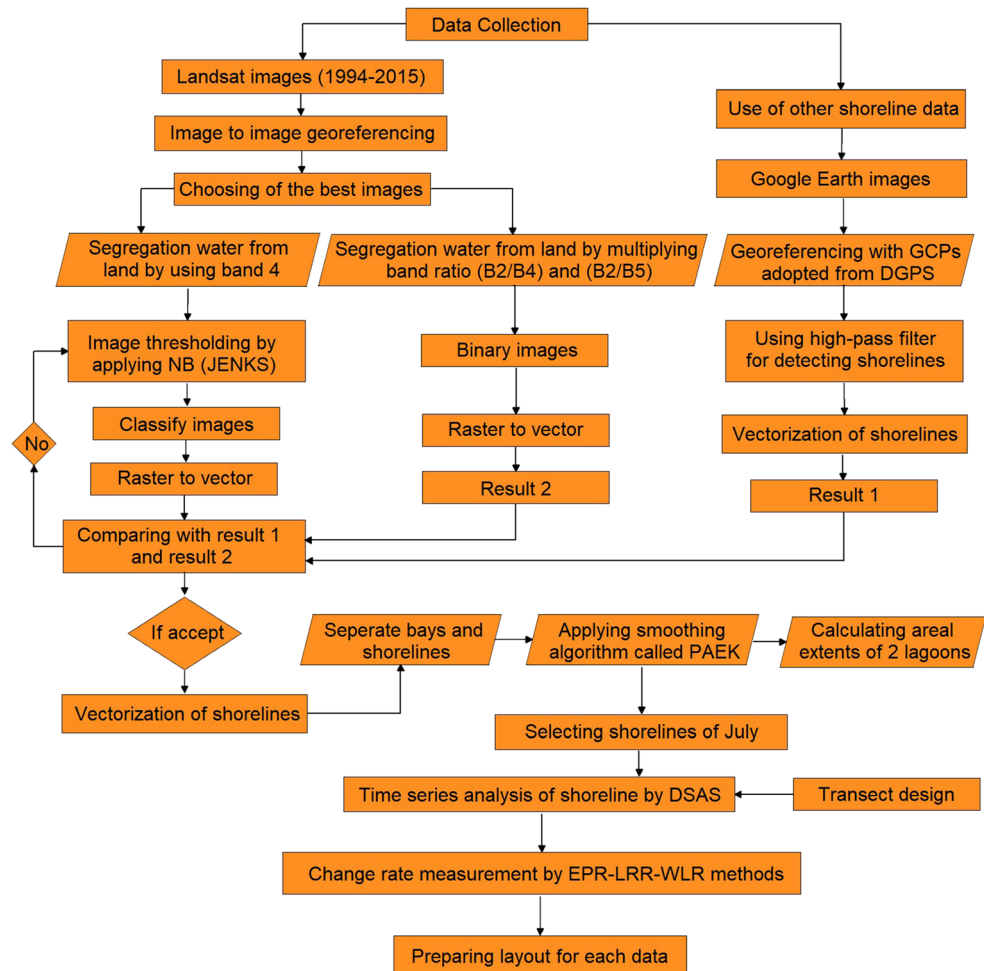


Fig. 5 Schematic of the methodology used for analyzing satellite images



The procedure includes four steps: (1) collecting shoreline data, (2) baseline construction, (3) transect generation, and (4) shoreline movement calculation (Thieler et al. 2009). Transects that are cast perpendicular to the baseline are used to establish measurement points for rate calculations. A hypothetical baseline was created to detect the spatiotemporal dynamics of shoreline evolution trends, similar to the general trend of the shoreline's geometry. Rates of shoreline change were calculated from shore-normal transects spaced at 250 m intervals along the coast. This transect resolution was found to be suitable to determine patterns of shoreline change in the study area. Based on the setting, a total of 304 and 152 transects were generated for the 76 km-long stretch of the Amirabad Coastline and Miankaleh Spit and a 38 km length along the Gomishan Lagoon. Estimations were performed by applying the three most commonly used statistical approaches: EPR, LRR, and WLR. The EPR method uses only two data points (the oldest and most recent shoreline positions) to determine a change rate. The information contained in the other data points is entirely ignored,

and therefore important trends or changes in trend may not be detected or incorporated into the results (Dolan et al. 1991; Genz et al. 2007). The LRR approach calculates the best fit line using the least-squares method for the whole data period. The slope of the line shows the rate of change for the shoreline. Since the line fit does not incorporate each data point's uncertainty, the method is susceptible to outlier effects. In WLR, data points with higher uncertainty will have less influence on the trend line than data points with smaller uncertainty. Like the LRR, this approach is sensitive to outliers even if their weights are small (Genz et al. 2007; Thieler et al. 2009).

Results and discussion

Shoreline evolution

Shorelines derived from Landsat imagery were analyzed to determine the evolution between different intervening periods and in different areas within the study region.

Shoreline locations at different times during the study period and rates of shoreline change (positive for shoreline progression and negative for recession) along all transects of each coastal zone are provided in Figs. 6 and 7. The calculated measures of change obtained by the three statistical approaches (EPR, LRR, and WLR) show similar values in most Amirabad and Miankaleh coastal zones (Fig. 6). In this portion of the CS coast, the mean rate of shoreline movement varies from -61.9 m/year (inside the Amirabad Port basin) to 55.3 m/year (close to the Miankaleh Spit terminus). While 11% of transects exhibit erosion, 89% of transects record deposition.

Along the Amirabad Coastline (distance 0–25,000 m in Fig. 6), where port structures obstruct littoral sediment transport, the natural equilibrium beach profile is disturbed. On the up-drift side of the breakwaters, excessive accretion and advancement of the shoreline are observed, while on the down-

drift side, erosion and retreat of the shoreline occurred. The accretion pattern is almost spatially uniform for the western and central parts of the Miankaleh Spit (distance 25,000–56,000 m in Fig. 6), with a mean progradation rate of 5.4 m/year, while substantial progradation occurred in the eastern part of the spit (more than 40 m/year at the distance 56,000–76,000 m).

The shoreline evolution results of the Gomishan area indicate a large-scale accretion pattern along the entire shoreline, and no erosion was detected for the studied period (Fig. 7). The LRR and WLR results generally agree, whereas the rates calculated by EPR are quite different. This could be attributed to the discrepancy in the theoretical bases of these methods and severe retreatment of shoreline position in 2015. Rates of shoreline change vary significantly along the Gomishan coast (Fig. 7). An average shoreline change rate of 92 m/year has been

Fig. 6 Calculated shoreline rates of change (m/year) based on three methods along the Amirabad and Miankaleh coastlines

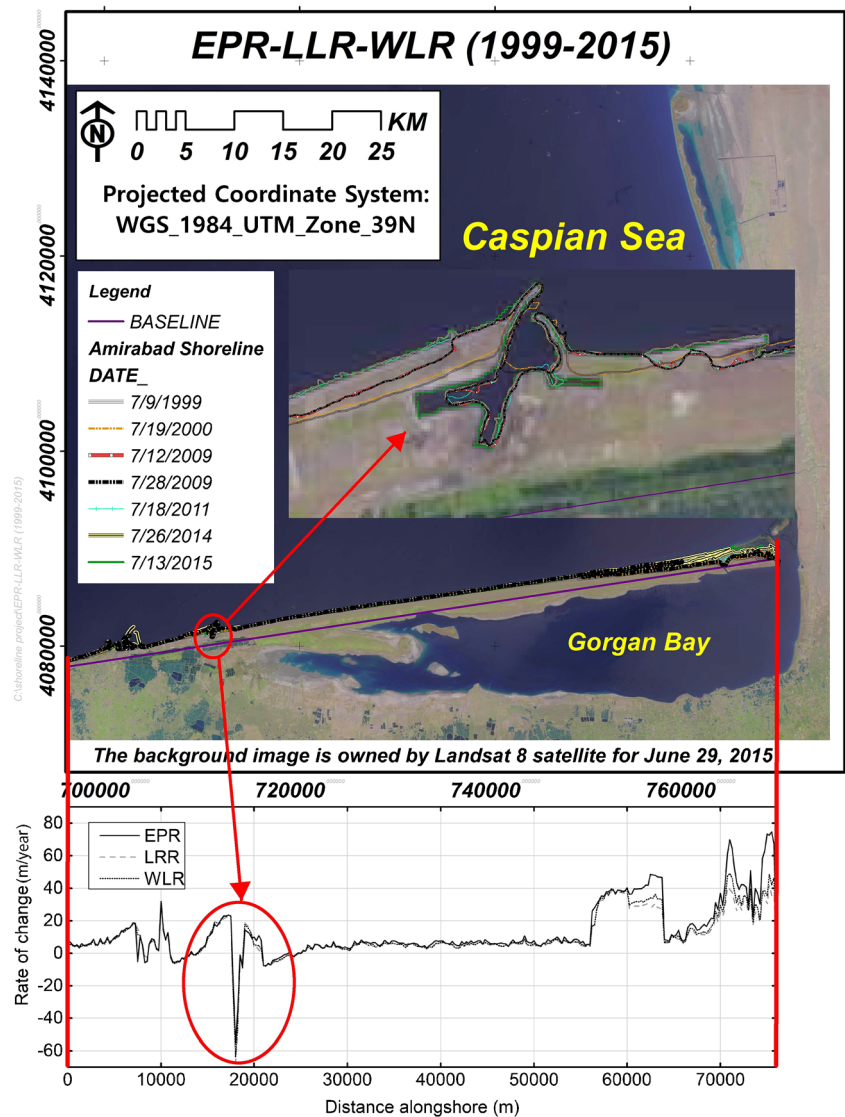
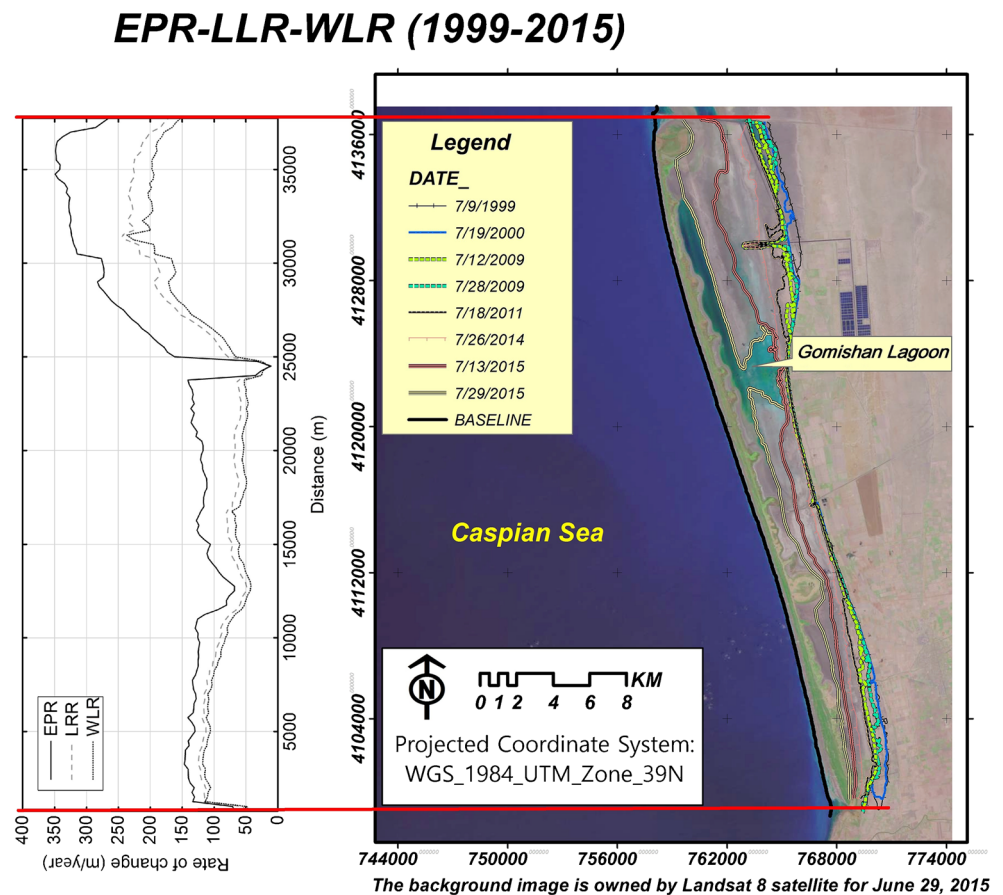


Fig. 7 Calculated shoreline rates of change (m/year) based on three methods along the Gomishan coastline



calculated for the southern and central parts of the lagoon and reaches 212 m/year in the northern part (distance 25,000–38,000 m in Fig. 7). The minimum accretion rate of 12.7 m/year was observed close to the beginning of the lagoon's northern part (distance 24,500 m). The highest values of progradation rates occurred in the northern portion of the lagoon (distance 30,000–38,000 m in Fig. 7).

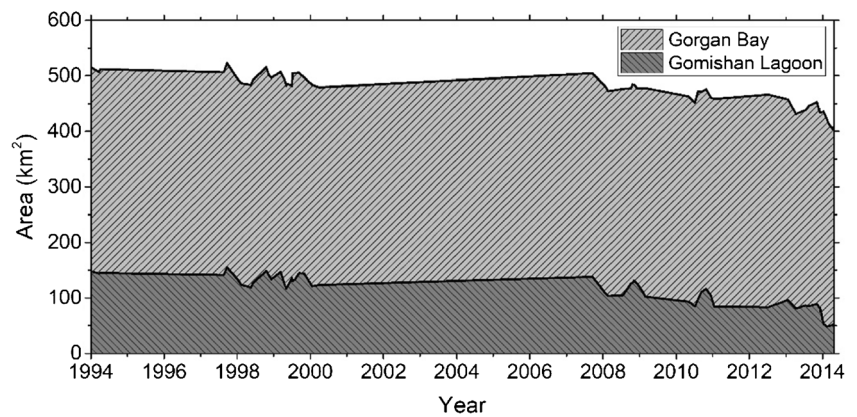
Both natural and anthropogenic causes influence shoreline position and control erosion-accretion on the beaches in the study area. The mild slope of the coastal profile over the eastern part of the study area, including the eastern part of the Miankaleh Spit and the entire Gomishan area, as well as accelerated water level drop in the CS, result in seaward progradation of the shoreline at an unexpected rate that causes emergence of extensive mudflats.

Shoreline movement is partly due to human intervention. Shoreline position around Amirabad, on both sides of the port, has locally prograded since 2000, after adjacent beaches were armored with hardened structures (revetment-seawalls) and a new phase of port development began. Construction of a new harbor basin within the port is responsible for the significant negative shoreline changes at Amirabad (Fig. 6).

Changes in the spit-lagoon complexes

Gorgan Bay was formed during the Neocaspian/Holocene period by an extended sandy spit called the Miankaleh coastal barrier system, which separates the bay from the sea (Svitoch and Yanina 2006). During sea level drop in the CS, the bay surface area decreased to 323 km² in 1975 (Kakroodi et al. 2012). When CS water level rose, Gorgan Bay grew to cover an area of ~ 523 km² in 1998. Since 1998, contemporaneous with sea level changes, the bay surface area has demonstrated a dynamic trend (Fig. 8). The areal extent of the bay reduced to ~ 372 km² in 2015, a ~ 151 km² loss compared to 1998. North of the Gorgan Bay in the Gomishan area, older lagoons such as Hassan Gholi Bay dried out during the rapid sea level drop between 1929 and 1977 (Kakroodi et al. 2012). With the rising water level after 1977, the new, shallow Gomishan Lagoon formed parallel to the shoreline at a lower elevation than previous lagoons (Kakroodi et al. 2015). The calculated changes in the areal extent of Gomishan Lagoon are very similar to the evolutionary trend of Gorgan Bay (Fig. 8). The surface area of Gomishan Lagoon was around 148 km² in 1994, reached

Fig. 8 Variations in the areal extent of spit-lagoon systems within the study area during 1994–2015



up to 155 km² in 1998, then decreased drastically to ~ 50.5 km² in 2015. The trend in morphological changes and the lagoon's areal extent during recent years show a remarkable shrinkage of the lagoon (Fig. 9). The regression analysis of the resulting areal changes in this study showed significant decreases in Gorgan Bay and Gomishan Lagoon's area, while the area of the Miankaleh Spit increased (Fig. 10). Gorgan Bay and Gomishan Lagoon decreased by 3.96 km²/year and 4.79 km²/year, respectively, over 22 years (Table 1). As illustrated in Fig. 11, the most considerable changes occurred in recent years due to the accelerated water level drop of the CS.

Morphological changes of the Miankaleh Spit

Spits shape and prograde in the direction of dominant littoral drift (Evans 1942). The most prominent morphological feature in the southeastern CS is the Miankaleh Spit, with an approximate west-east length of 60 km (Kakroodi et al. 2012). The spit developed due to strong eastward longshore sediment transport and has a relatively straight alignment. It is crenulated on its bayside but smooth along the seaward edge. The spit is open on the eastern tip close to the Gorgan River delta and is connected to the mainland on the west at the Amirabad coastal zone. Investigation of the morphological changes of the spit indicates significant growth in the areal extent (Fig. 12) attributed to water level drop in the CS and nearshore processes. The overall rate of change in the surface area of Miankaleh Spit is calculated with respect to the 1994 shoreline position as the base year using the LRR method of estimation (Table 1). The spit is growing eastwards and increasing in size at a rate of 2.007 km²/year. Gradual eastward progression of Miankaleh Spit leads to blocking and limiting the remaining open inlets at its easternmost

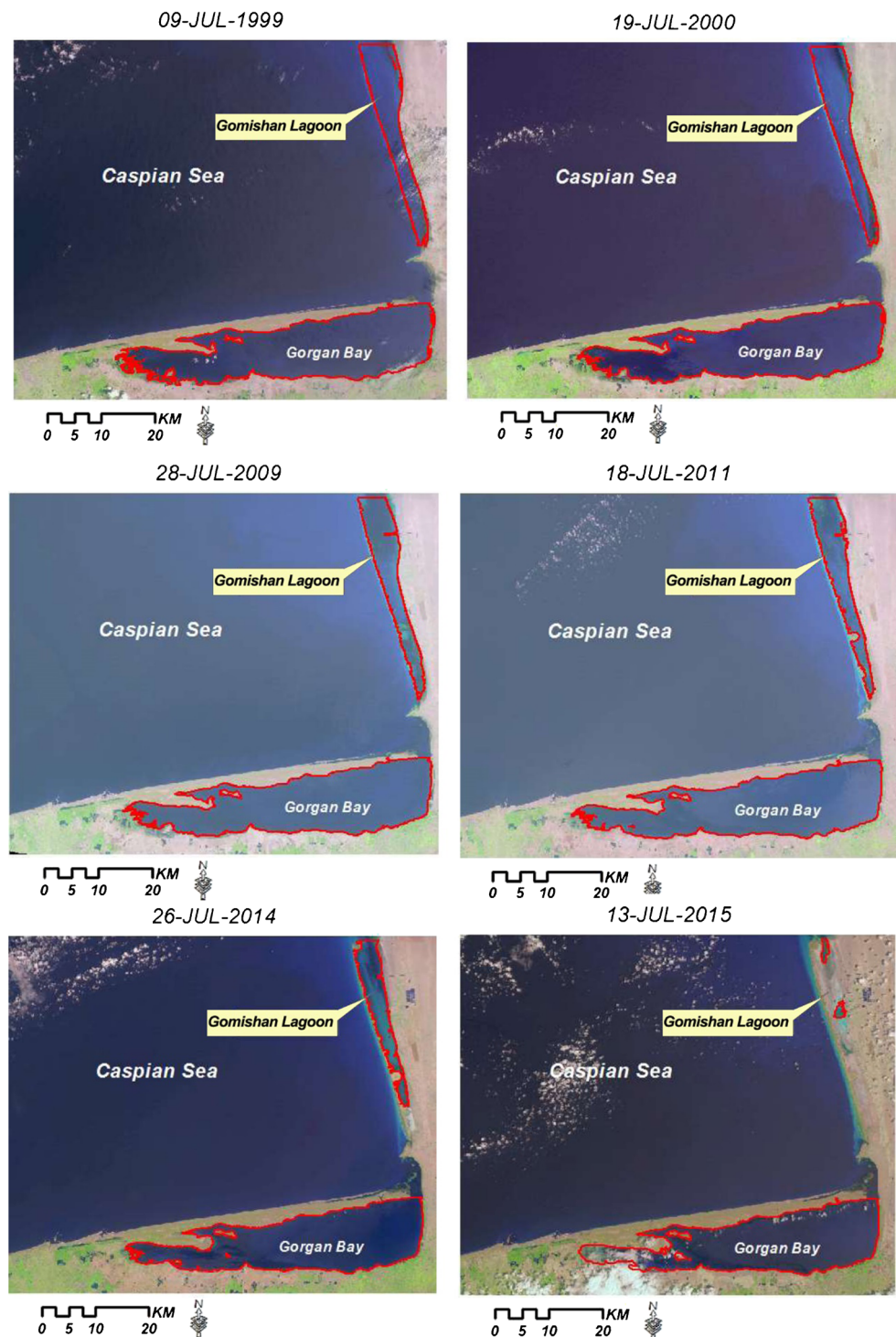
end and compromises Gorgan Bay's connection with the CS (Fig. 13).

Although the analyses presented in this paper are based on the satellite images taken by the year 2015, images acquired between 2015 and 2019 show a similar rate of areal change for Gorgan Bay, Gomishan Lagoon, and Miankaleh Spit as in 1994–2015. This consistency could be due to the continued drop in water level in the CS since 2015, although the rate of decrease is smaller than the study period. Water level measurements at Anzali station show that the water level in December 2019 was about -27.3 m, 0.20 m lower than in 2015, showing that the trend of water level variation between 2015 and 2019 was similar to that in the study period. Therefore, the area of Gorgan Bay and Gomishan Lagoon would decrease and the length of the Miankaleh Spit would increase. Indeed, satellite images from 2019 show this happening. The Landsat 8 image taken on August 25, 2019 shows that the Miankaleh Spit has progressed further east since 2015 (Fig. 14a). The connection between the CS and the Gorgan Bay has been limited to two narrow inlets (Fig. 14b) due to greater water level drop than in 2015. The areal extent of the Gorgan Bay and Gomishan Lagoon seems similar to 2015. It is worth nothing that in April 2019, an intense flood affected the Gomishan and, to some extent, the Miankaleh region and temporarily (for several weeks) increased the areal extent of Gomishan Lagoon. However, after the flood receded, the bay area shrank again, which demonstrates that its area is controlled by CS water level.

The role of coastal processes on morphological changes of the Miankaleh Spit

In the previous sections, the long-term and annual rates of change in the lagoons' and the spit's area were calculated based on time series of satellite image analysis. These

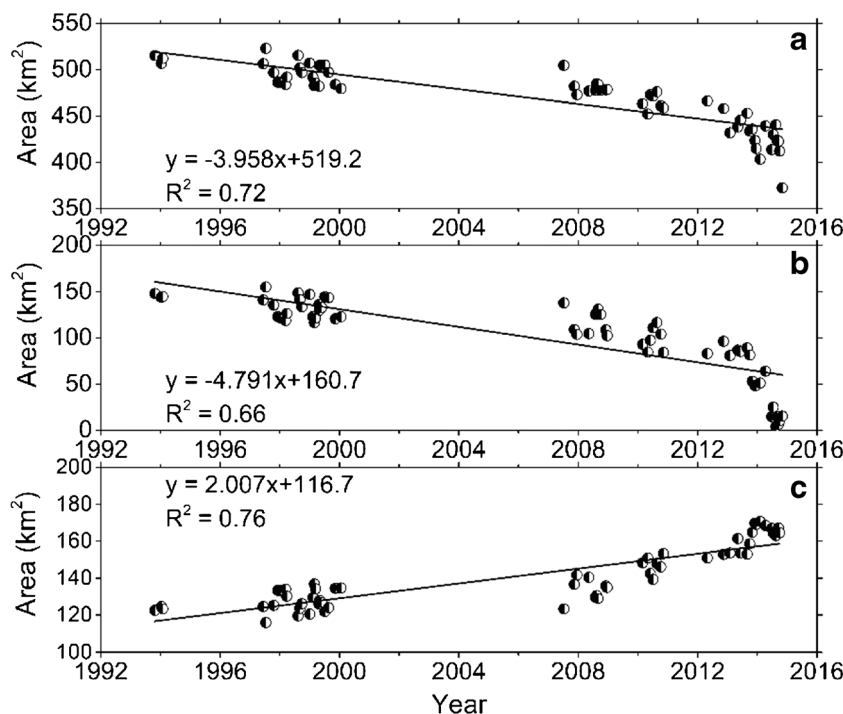
Fig. 9 Areal changes of the spit-lagoon complexes in the study region. Most of the changes occurred during recent years, contemporaneously with the Caspian Sea level drop



rates account for the combined effect of CS water level fluctuations and other effects, including longshore sediment transport. In the case of Gorgan Bay and especially Gomishan Lagoon, the variations in area can almost completely be attributed to water level changes, because

these regions are partially or entirely isolated from the CS; therefore, littoral drift cannot affect the inner morphological features. Miankaleh Spit is a different case, since its northern side is affected by waves and littoral drift of the CS. Examining wind data from the European Centre

Fig. 10 Plots of areal extent (y-axis) versus time (x-axis) for **a** Gorgan Bay, **b** Gomishan Lagoon, and **c** Miankaleh Spit. In the regression equations, x is the difference between the study year and 1994 as the origin year of the investigation



for Medium-Range Weather Forecasts (ECMWF) during the period 1992–2003 along with the wave simulation results from the Iranian Seas Wave Modeling project (ISWM) database (Allahdadi et al. 2004) shows that in the southeastern CS, wind and wave conditions favor a dominant littoral drift from west to east (Fig. 15).

To examine the effect of waves on coastal currents and littoral drift along the Miankaleh Spit, wave propagation and the corresponding alongshore currents along the spit were simulated using Mike 21 (DHI 2014). The results show that the alongshore currents under the dominant wave directions from the northwest (in the coastal area with depth up to 5 m; see Fig. 16a for bathymetry) have a general direction of west to east along the spit. For the Gomishan Lagoon coastline, the general current direction is from north to south (Fig. 16b and c). Simulations also show that at the eastern tip of the spit, both west-east and

north-south longshore currents significantly weaken because of the substantial decline in wave height. Therefore, currents lose sediment carrying power, causing sedimentation at the Gorgan Bay entrance and the tip of Miankaleh Spit. To quantify the contribution of longshore sediment transport (LST) on the evolution of Miankaleh Spit, we conservatively assumed that the whole LST along the spit contributes to the elongation of the spit at the eastern tip. Based on the dominant northwest wave direction offshore of the Miankaleh Spit and the specific

Table 1 Relationships for the morphological changes of selected regions versus time, based on the LRR method, during 1994–2015. The equation is $y = mx + b$, where y is the areal extent with 1994 as a base year, m represents the rate of change, b is a constant representing the y-intercept, and R^2 represents coefficient of determination

Coastal zone	Physical extent	m	b	R^2
Gorgan Bay	Area (km ²)	-3.958	519.2	0.72
Gomishan Lagoon	Area (km ²)	-4.791	160.7	0.66
Miankaleh Spit	Area (km ²)	2.007	116.7	0.76

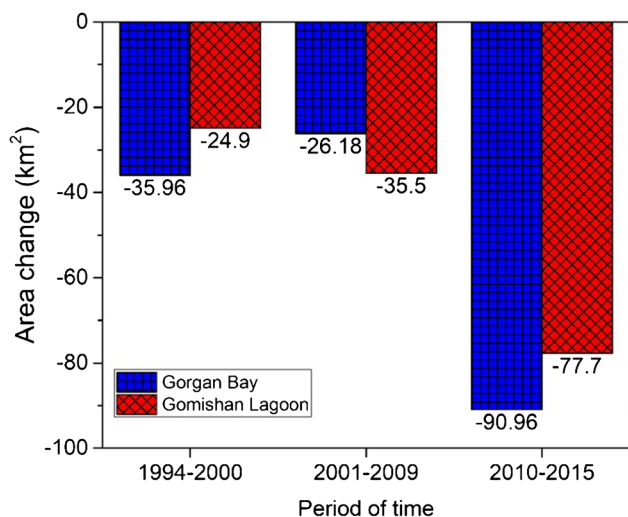
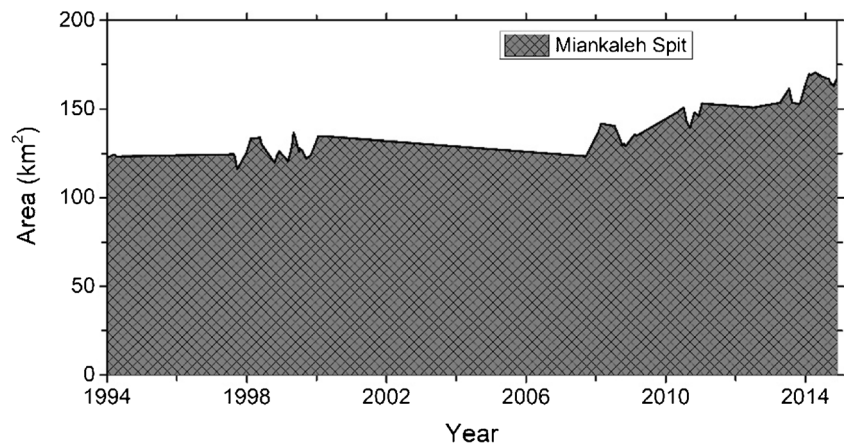


Fig. 11 Changes in surface area in the study region over the specified periods

Fig. 12 Variations in the areal extent of Miankaleh Spit between 1994 and 2015

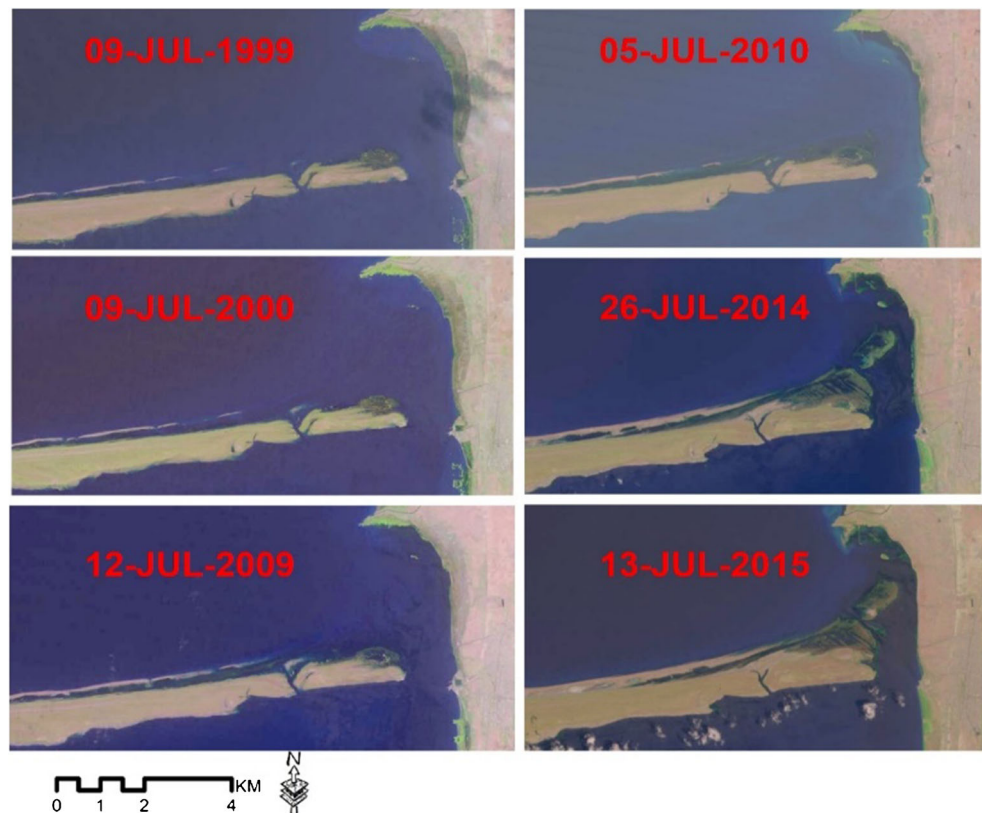


alignment of the spit, the net west-to-east rate of LST was calculated as $80,000 \text{ m}^3/\text{year}$ by Gharibreza et al. (2018). Also, the results from satellite image analysis (Fig. 12) show that the total increase in the areal extent of the spit from 1994 to 2015 was 41.14 km^2 . Considering the total sea level drop of 1.31 m during this period (Fig. 3), the annual volume of spit elongation would be $1,314,000 \text{ m}^3$. Dividing the annual net LST rate of $80,000 \text{ m}^3$ by this amount shows an annual contribution of 6% from LST in the evolution of Miankaleh Spit.

Conclusions

Spatiotemporal dynamics of beach evolution in the south-eastern Caspian Sea (CS) have been successfully examined by analyzing Landsat images (satellites 4, 5, 7, and 8) between 1994 and 2015 and employing a histogram thresholding procedure as well as band ratio method for shoreline extraction. Computations of change rates of shoreline position and physical extent of study areas have been performed using statistical approaches. Detailed

Fig. 13 Miankaleh Spit growth at different dates as a consequence of CS sea level drop and eastward alongshore sediment transport



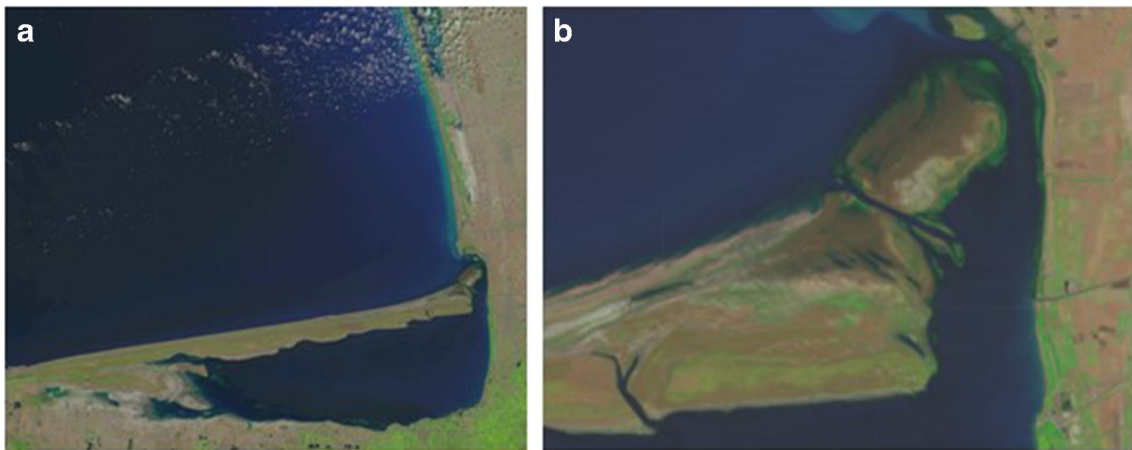


Fig. 14 **a** True color Landsat 8 image of the study area acquired on 25 August 2019 showing the eastward progression of the Miankaleh Spit. **b** The magnified image of the Gorgan Bay entrance

analysis of historical and contemporary shoreline changes reveals highly variable accretion patterns along the entire shoreline of the study area except in part of the Amirabad coastal region, where an erosional trend is apparent due to anthropogenic activities. By comparing the performance of three computational methods, we conclude that EPR, the most widely used method for shoreline extraction, can result in unreliable values in coastal areas exposed to large temporal variability (such as in the Gomishan area). The LRR and WLR methods were the most appropriate methods for estimating the long-term shoreline change rate within selected areas in this study.

Our findings suggest that morphological changes and coastal variability in the study area are primarily affected by water level

fluctuations in the CS. Following rising CS water levels, both Gorgan Bay and Gomishan Lagoon increased in size; declining CS water levels resulted in a reduction in their size. Development of the Miankaleh Spit both in length and width is attributed to the water level drop in the CS and nearshore processes. The estimated contribution of the littoral drift in elongation of the spit is ~6% of the total annual elongation rate calculated from satellite images and the estimated annual rate of longshore sediment transport at the tip of the spit. Gorgan Bay is at risk of disconnecting with the CS due to the eastward progradation of the spit. Overall, beach evolution has increased in the study area during recent years due to accelerated water level drop in the CS. The southeastern CS coastal zone exhibits a high rate of coastal evolution compared to other Iranian Caspian coastal zones (Kakroodi et al. 2012).

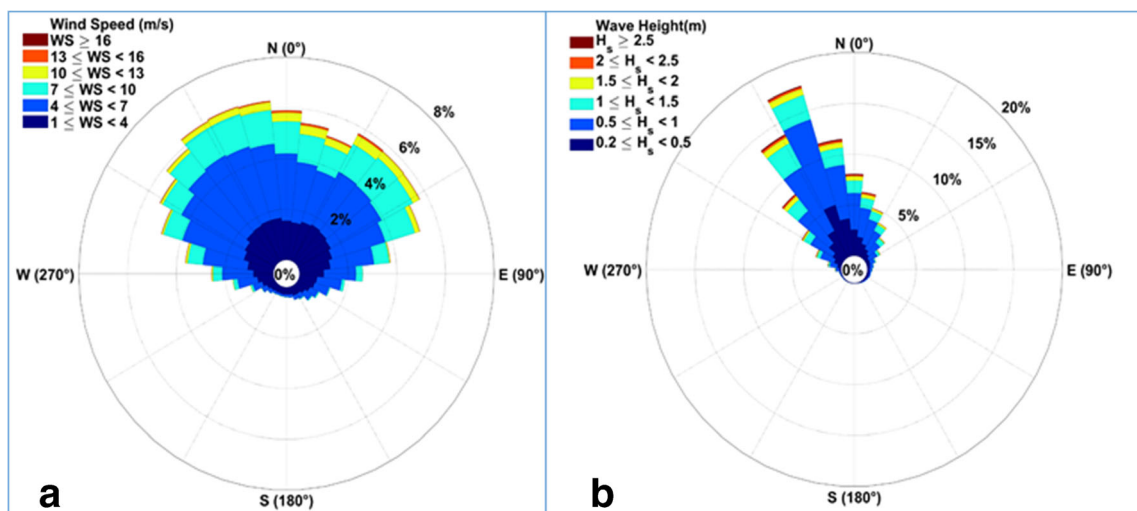
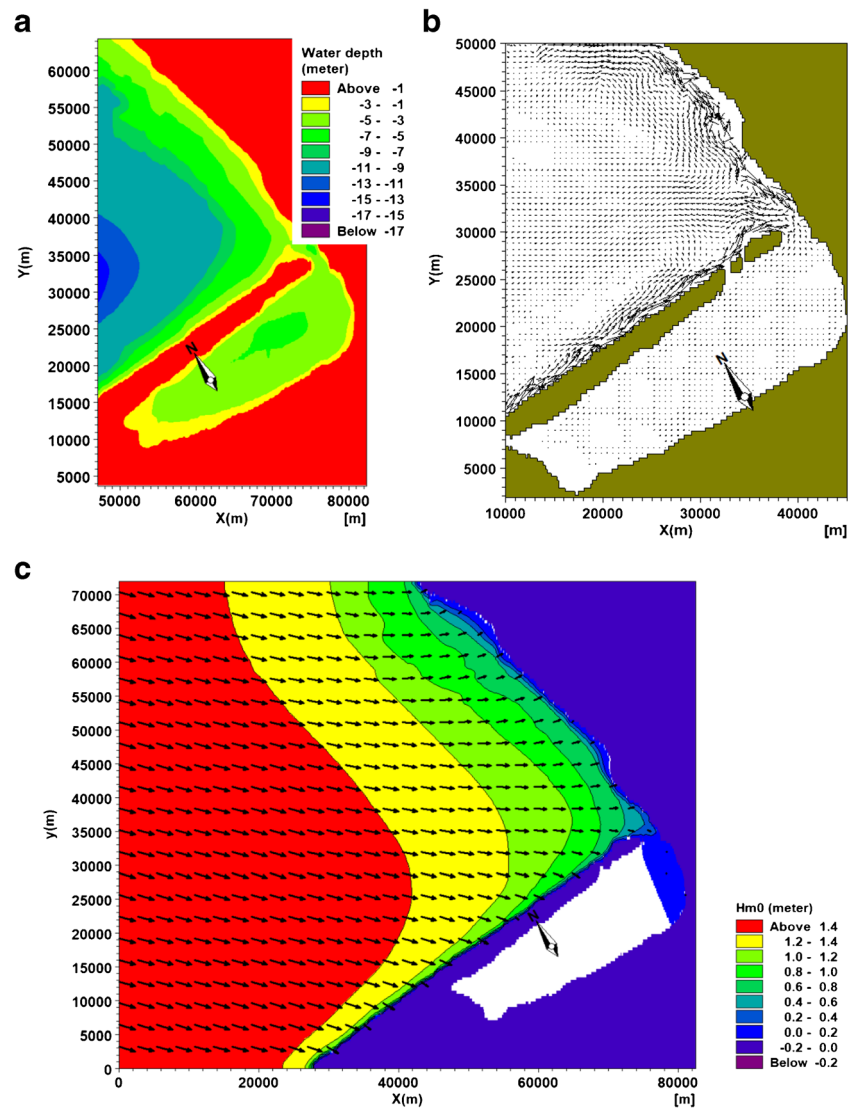


Fig. 15 **a** ECMWF wind rose and **b** ISWM wave rose (Allahdadi et al. 2004) at a location offshore of the Miankaleh Spit (longitude = 53.125° E, latitude = 37.375° N)

Fig. 16 **a** Bathymetry of the southeastern CS, including the Gorgan Bay and Miankaleh Spit. **b** Simulated alongshore currents generated by waves from the northwest (330°) with a height of 1.5 m. **c** Wave propagation pattern corresponding to a wave height of 1.5 m from 330° . Due to computational concerns in Mike 21, the modeling area and the results were all rotated 30° counterclockwise (notice the north arrow)



Our study also illustrates that remotely sensed data, GIS techniques, and numerical simulation provide valuable information for analysis of short- and long-term coastal changes in response to various factors that can be valuable in coastal zone management.

Acknowledgements The authors appreciate the Iranian Port and Maritime Organization (PMO) for sharing the ECMWF wind data and the simulation wave data from the ISWM project for the study area. We thank the N.F.T. Company for providing the licensed version of the Mike 21 model for simulation of waves and current. We also thank Jennifer Warrillow for the help with the manuscript.

Declarations

Conflict of interest The authors declare that they have no competing interests.

References

- Aedla R, Dwarakish GS, Venkat Reddy D (2015) Automatic shoreline detection and change detection analysis of Netravati-Gurpur River mouth using histogram equalization and adaptive thresholding techniques. *Aquat Procedia* 4:563–570. <https://doi.org/10.1016/j.aqpro.2015.02.073>

- Alizadeh Ketek Lahijani H, Tavakoli V, Amini AAH (2008) South Caspian river mouth configuration under human impact and sea level fluctuations. *Environ Sci* 5(2):65–86
- Allahdadi MN, Chegini V, Fotouhi N, Golshani A (2004) Wave modeling and hindcast of the Caspian Sea. Abstract in proceeding of 6th international conference on coasts, ports, and marine structures, Tehran, I.R. Iran
- Bartlett D, Smith J (2004) GIS for coastal zone management. CRC Press, Boca Raton, London, New York, Washington, D.C.
- Boak EH, Turner IL (2005) Shoreline definition and detection: a review. *J Coast Res* 21(4):688–703. <https://doi.org/10.2112/03-0071.1>
- Chaichitehrani N, Li C, Xu K, Allahdadi MN, Hestir EL, Keim BD (2019) A numerical study of sediment dynamics over Sandy Point dredge pit, west flank of the Mississippi River, during a cold front event. *Cont Shelf Res* 183:38–50. <https://doi.org/10.1016/j.csr.2019.06.009>
- DHI water and environment (2014) Mike 21 user manual, Denmark
- Dolan R, Fenster MS, Holme SJ (1991) Temporal analysis of shoreline recession and accretion. *J Coast Res* 7(3):723–744. <https://www.jstor.org/stable/4297888>. Accessed 20 April 2021
- Evans OF (1942) The origin of spits, bars, and related structures. *J Geol* 50(7):846–865. <https://www.jstor.org/stable/30062605>. Accessed 20 April 2021
- Firoozfar A, Bromhead EN, Dykes AP, Lashte Neshaei MA (2012) Southern Caspian Sea coasts, morphology, sediment characteristics, and sea level change. Abstract in proceeding of the annual international conference on soils, sediments, water and energy
- Genz AS, Fletcher CH, Dunn RA, Frazer LN, Rooney JJ (2007) The predictive accuracy of shoreline change rate methods and along-shore beach variation on Maui, Hawaii. *J Coast Res* 231:87–105. <https://doi.org/10.2112/05-0521.1>
- Gharibreza M, Nasrollahi A, Afshar A, Amini A, Eisaei H (2018) Evolutionary trend of the Gorgan Bay (southeastern Caspian Sea) during and post the last Caspian Sea level rise. *Catena* 166:339–348. <https://doi.org/10.1016/j.catena.2018.04.016>
- Ibrayev RA, Özsoy E, Schrum C, Sur Hİ (2010) Seasonal variability of the Caspian Sea three-dimensional circulation, sea level and air-sea interaction. *Ocean Sci* 6(1):311–329. <https://doi.org/10.5194/os-6-311-2010>
- Isaie Moghaddam E, Hakimzadeh H, Allahdadi MN, Hamed A, Nasrollahi A (2018) Wave-induced currents in the northern Gulf of Oman: a numerical study for Ramin Port along the Iranian coast. *Am J Fluid Dyn* 8(1):30–39. <https://doi.org/10.5923/j.ajfd.20180801.04>
- Kakroodi AA, Kroonenberg SB, Hoogendoorn RM, Mohamm Khani H, Yamani M, Ghassemi MR, Lahijani HAK (2012) Rapid Holocene sea-level changes along the Iranian Caspian coast. *Quat Int* 263:93–103. <https://doi.org/10.1016/j.quaint.2011.12.021>
- Kakroodi AA, Kroonenberg SB, Goorabi A, Yamani M (2014) Shoreline response to rapid 20th century sea-level change along the Iranian Caspian coast. *J Coast Res* 30(6):1243–1250. <https://doi.org/10.2112/JCOASTRES-D-12-00173.1>
- Kakroodi AA, Leroy SAG, Kroonenberg SB, Lahijani HAK, Alimohammadian H, Boomer I, Goorabi A (2015) Late Pleistocene and Holocene sea-level change and coastal paleoenvironment evolution along the Iranian Caspian shore. *Mar Geol* 361:111–125. <https://doi.org/10.1016/j.margeo.2014.12.007>
- Kaplin PA, Selivanov AO (1995) Recent coastal evolution of the Caspian Sea as a natural model for coastal responses to the possible acceleration of global sea-level rise. *Mar Geol* 124(1–4):161–175. [https://doi.org/10.1016/0025-3227\(95\)00038-Z](https://doi.org/10.1016/0025-3227(95)00038-Z)
- Kermani S, Boutiba M, Guendouz M, Guettouche MS, Khelfani D (2016) Detection and analysis of shoreline changes using geospatial tools and automatic computation: case of jijelian sandy coast (East Algeria). *Ocean Coast Manag* 132:46–58. <https://doi.org/10.1016/j.ocecoaman.2016.08.010>
- Kosarev AN, Tuzhilkin VS, Kostianoy AG (2012) Main features of the Caspian Sea hydrology. In: Nihoul JCJ, Zavialov PO, Micklin PP (eds) Dying and dead seas climatic versus anthropic causes. NATO science series: IV: earth and environmental sciences, vol 36. Springer, Dordrecht, pp 159–184. https://doi.org/10.1007/978-94-007-0967-6_7
- Kourosh Niya A, Alesheikh AA, Soltanpor M, Kheirkhahzarkesh MM (2013) Shoreline change mapping using remote sensing and GIS. *Int J Remote Sens Appl* 3(3):102–107
- Kuleli T, Guneroglu A, Karsli F, Dihkan M (2011) Automatic detection of shoreline change on coastal Ramsar wetlands of Turkey. *Ocean Eng* 38(10):1141–1149. <https://doi.org/10.1016/j.oceaneng.2011.05.006>
- Lahijani H (1997) Riverine sediments and stability of Iranian coast of the Caspian Sea. Ph.D. Dissertation. Russian Academy of Sciences, Moscow, Russia
- Lahijani HAK, Rahimpour-Bonab H, Tavakoli V, Hosseindoost M (2009) Evidence for late Holocene highstands in central Guilan-east Mazanderan, south Caspian coast, Iran. *Quat Int* 197(1–2):55–71. <https://doi.org/10.1016/j.quaint.2007.10.005>
- Lebedev SA (2004) Investigation of seasonal and interannual variability of the Caspian Sea level and Volga River run-off by satellite TOPEX/Poseidon and Jason-1 altimetry data. Abstract in proceeding of 35th COSPAR scientific assembly, Paris, France
- Lebedev SA, Ostroumova LP, Sirota AM (2008) Seasonal and interannual variability of the Caspian Sea evaporation on remote sensing data. Abstract in proceeding of EGU general assembly, Vienna, Austria
- Lepeshevkov IN, Buynevich DV, Buynevich NA (1981) Perspectives of use of the Kara-Bogaz-Gol salt resources. *Nayka*, Moscow, p 274 (in Russian)
- Leroy SAG, Wamy S, Lahijani H, Piovano EL, Fanetti D, Berger AR (2009) The role of geosciences in the mitigation of natural disasters: five case studies. *Geophys Hazards*:115–147. https://doi.org/10.1007/978-90-481-3236-2_9
- Liu Y, Huang H, Qiu Z, Fan J (2013) Detecting coastline change from satellite images based on beach slope estimation in a tidal flat. *Int J Appl Earth Obs* 23(1):165–176. <https://doi.org/10.1016/j.jag.2012.12.005>
- Naderi Beni A, Lahijani H, Moussavi Harami R, Leroy SAG, Shah-Hosseini M, Kabiri K, Tavakoli V (2013) Development of spit-lagoon complexes in response to Little Ice Age rapid sea-level changes in the central Guilan coast, south Caspian Sea, Iran. *Geomorphology* 187:11–26. <https://doi.org/10.1016/j.geomorph.2012.11.026>
- Pourmandi Yekta AH, Ardalan H, Babaee M (2010) Caspian Sea hydrodynamic characteristics in Amirabad Neka coastal area. Abstract in proceeding of 9th international conferences on coasts, ports and marine structures, Tehran, I.R. Iran
- Rasuly A, Naghdifar R, Rasoli M (2010) Monitoring of Caspian Sea coastline changes using object-oriented techniques. *Procedia Environ Sci* 2:416–426. <https://doi.org/10.1016/j.proenv.2010.10.046>
- Rychagov GI (1997) Holocene oscillations of the Caspian Sea, and forecasts based on palaeogeographical reconstructions. *Quat Int* 41–42: 167–172. [https://doi.org/10.1016/S1040-6182\(96\)00049-3](https://doi.org/10.1016/S1040-6182(96)00049-3)
- Svitoch AA, Yanina TA (2006) Holocene marine sediments on the Iranian coast of the Caspian Sea. *Dokl Earth Sci* 410(7):1166–1169. <https://doi.org/10.1134/S1028334X06070373>
- Terziev SF (1992) Hydrometeorology and hydrochemistry of seas, the Caspian Sea. In: *Hydrometeorological conditions* 6: 360, Gidrometeoizdat, Leningrad
- Thieler ER, Himmelstoss EA, Zichichi JL, Ergul A (2009) The digital shoreline analysis system (DSAS) version 4.0 - an ArcGIS extension for calculating shoreline change. <https://doi.org/10.3133/ofr20081278>

- USDA (2015) https://ipad.fas.usda.gov/cropexplorer/global_reservoir/. Last accessed 12.Feb. 2020
- Vinayaraj P, Johnson G, Udhaba Dora G, Sajiv Philip C, Sanil Kumar V, Gowthaman R (2011) Quantitative estimation of coastal changes along selected locations of Karnataka, India: a GIS and remote sensing approach. *Int J Geosci* 2(4):385–393. <https://doi.org/10.4236/ijg.2011.24041>
- Voropaev GV, Krasnozhan GE, Lahijani H (1998) Riverine sediments and stability of the Iranian coast of the Caspian Sea. *Water Resour* 25(6):747–758
- Zuzek PJ, Nairn RB, Thieme SJ (2003) Spatial and temporal considerations for calculating shoreline change rates in the Great Lakes Basin. *J Coast Res* 38:125–146. <http://www.jstor.org/stable/25736603>. Accessed 20 April 2021